SCIENCE CHINA
Information Sciences

• RESEARCH PAPER •

April 2016, Vol. 59 042405:1–042405:10
doi: 10.1007/s11432-015-5400-0

Novel wavelet neural network algorithm for continuous and noninvasive dynamic estimation of blood pressure from photoplethysmography

Peng LI, Ming LIU*, Xu ZHANG*, Xiaohui HU, Bo PANG,
Zhaolin YAO & Hongda CHEN

State Key Laboratory on Integrated Optoelectronic, Institute of Semiconductors, Chinese Academy of Sciences, Beijing 100083*, China*

Received May 10, 2015; accepted June 18, 2015; published online September 25, 2015

Abstract This paper proposes a novel wavelet neural network algorithm for the continuous and noninvasive dynamic estimation of blood pressure (BP). Unlike prior algorithms, the proposed algorithm capitalizes on the correlation between photoplethysmography (PPG) and BP. Complete BP waveforms are reconstructed based on PPG signals to extract systolic blood pressure (SBP) and diastolic blood pressure (DBP). To improve the robustness, Daubechies wavelet is implemented as the hidden layer node function for the neural network. An optimized neural network structure is proposed to reduce the computational complexity. Further, this paper investigates an inhomogeneous resilient backpropagation (IRBP) algorithm to calculate the weight of hidden layer nodes. The IRBP improves the convergence speed and reconstruction accuracy. Multiparameter intelligent monitoring in Intensive Care (MIMIC) databases, which contain a variety of physiological parameters captured from patient monitors, are used to validate this algorithm. The standard deviation σ between reconstructed and actual BP signals is 4.4797 mmHg, which satisfies the American National Standards of the Association for the Advancement of Medical Instrumentation. The reconstructed BP waveform can be used to extract the SBP and DBP, whose standard deviations σ are 2.91 mmHg and 2.41 mmHg respectively.

Keywords photoplethysmogram (PPG), blood pressure (BP), Daubechies wavelet, neural network, inhomogeneous resilient backpropagation (IRBP)

Citation Li P, Liu M, Zhang X, et al. Novel wavelet neural network algorithm for continuous and noninvasive dynamic estimation of blood pressure from photoplethysmography. Sci China Inf Sci, 2016, 59(4): 042405, doi: 10.1007/s11432-015-5400-0

1 Introduction

Blood pressure (BP) is an important parameter reflecting the performance of human circulatory system. Mankind is plagued by numerous diseases related to arterial blood pressure (ABP), including hypertension and heart disease. Because of the complex mechanisms of these diseases, they are difficult to cure. Countless scientists and clinicians are dedicated to identifying early warning indicators of these diseases. Therefore, physiological signals acquisition [1–5] and processing [6–9] have become widespread research topics in recent years.

* Corresponding author (email: liuming@semi.ac.cn, zhangxu@semi.ac.cn)

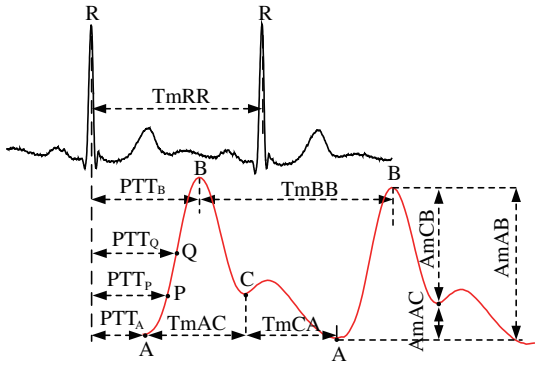

Figure 1 (Color online) Multi-feature extraction from ECG and PPG.

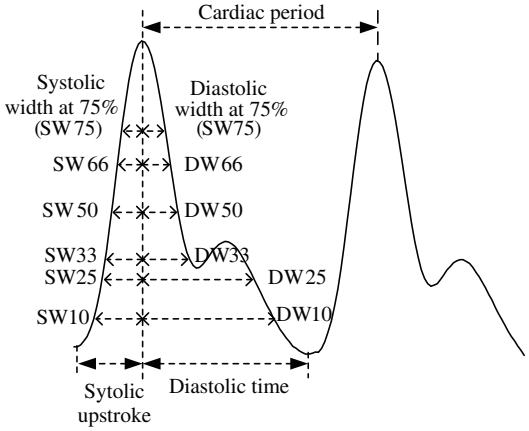

Figure 2 Multi-feature extraction from a single PPG.

Among these diseases, hypertension has a high incidence. The measurement of systolic blood pressure (SBP) and diastolic blood pressure (DBP) is meaningful for the prevention of hypertension. For this reason, portable electronic sphygmomanometers have become common. However, the usage of a cuff can cause discomfort to users, which may then reduce the measurement accuracy. Another disadvantage of this approach is that it is impossible to measure BP in real time.

Rather than using a cuff, researchers are attempting to measure BP by other methods such as, arterial tonometry [10] and pulse wave velocity (PWV) [11]. For arterial tonometry, many sensors are pressed onto the skin surface of arteries, which is not suitable for application. The measurement of PWV is an extremely complex process, where different mathematical models are established and the blood flow must be measured accurately. Fortunately, the pulse transit time (PTT) reported in [12] and [13] has a strong correlation with BP. Compared with arterial tonometry and PWV, the measurement of PTT is uncomplicated, requiring only two sensors. There are two typical methods to measure PTT. The first [14] is to calculate the delay between Electrocardiogram (ECG) and PPG, and the second method [15] is to measure the delay of different PPGs acquired from different parts of the body. To improve the accuracy of the evaluation of BP, a new feature vector extraction algorithm was proposed by Li et al. in [16]. As illustrated in Figure 1, the PPG is divided into different parts by amplitude. A group of PTTs and other feature vectors related to PPG are extracted. Experimental results demonstate that the correlation of BP and several feature vectors related to single PPG signals are as strong as those of BP and PTT. The estimation of BP through single PPG signals has been investigated in [17–19]. Compared with [12] and [13], only one sensor is needed by this approach, which reduces the hardware cost. Moreover, the alignment problem of different signals (ECG and PPG, PPG and PPG) is solved, which reduces the measurement error. Kurylyak et al. [20] proposed a neural network-based method for BP estimation from single PPG signals. The method of extracting feature vectors from PPG signals is presented in Figure 2.

These algorithms indicate that there is a strong correlation between PPG and BP. The number of sensors and data alignment are two key issues for estimating BP from multi-physiological parameters (ECG and PPG, PPGs). The single PPG method is a good solution for these issues. However, all these algorithms focus on the correlation between BP values (SBP and DBP) and feature vectors only. Robust performance is an implicit and main problem for these algorithms. The quality of feature vectors (PTTs and others) extracted from physiological parameters is strongly dependent on input signals (physiological parameters) acquired by sensors. If input signals are disturbed by noise, the quality of feature vectors will decline, reducing the estimation accuracy of the BP. For example, the notch of PPGs (C points) in Figure 1 is difficult to determine because of the noise interference.

To solve these problems, a novel wavelet neural network algorithm for BP estimation is proposed in this paper. Differing from previous algorithms, we do not extract feature vectors from the PPG. Complete

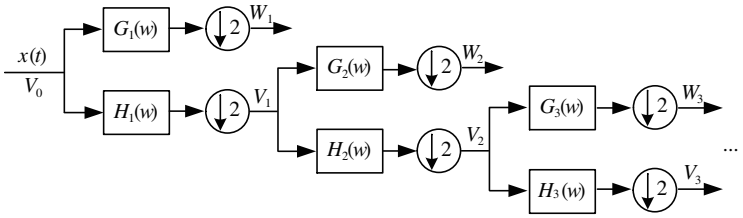

Figure 3 The input signal $x(t)$ is decomposed in the multi-dimensional frequency space

PPG signals are chosen as feature vectors. The complete correlation information between the PPG and BP is maintained. Complete BP signals are reconstructed and used to extract the SBP and DBP. In this manner, we avoid the noise interference of feature vector extraction and obtain accurate SBP and DBP.

The rest of this paper is organized as follows: Section 2 presents the theory of wavelet transform (WT) and the application of Daubechies wavelet. Section 3 discusses wavelet neural networks. The IRBP is proposed in Section 4. The experimental results are presented in Section 5. Our conclusions are made in Section 6.

2 Wavelet transform

WT refers to decomposing signals with finite length or fast decay of the oscillation waveform that is the mother wavelet $\psi(t)$. In general, $\psi(t)$ is the combination function of $\phi(t)$, which is the scale function or father wavelet. Its calculation expression is defined as

$$\phi(t) = \sqrt{2} \sum_{k \in Z} h_k \phi(2t - k), \tag{1}$$

$$\psi(t) = \sqrt{2} \sum_{k \in Z} g_k \psi(2t - k), \tag{2}$$

where h_k and g_k are a pair of equivalent filter coefficients (lowpass and highpass). The input signal $x(t)$ is decomposed by step as indicated in Figure 3. This is the main property of WT, the multi-resolution analysis. WT can analyze signals at different scales by adjusting filter types (low-pass, high-pass and band-pass). For different signals, we can adjust the scale function to acquire parts of interest. This is the primary reason that the wavelet is chosen as the node function of neural networks.

Daubechies wavelet is a kind of wavelet function named after Ingrid Daubechies [21]. The convergence property and the fact that it is compactly supported in frequency domain are advantages of the Daubechies wavelet [22]. It is used mainly in the discrete wavelet transform, especially in fast wavelet transform.

In this paper, MIMIC databases [23] are chosen as data sources. Original PPG signals and fast Fourier transform (FFT) spectrum analysis are presented in Figure 4(a) and (b) respectively. Clearly, the energy of PPG signals is mainly concentrated in the low frequency (below 20 Hz). Therefore, We fully use the low-pass filter feature of Daubechies wavelet. The frequency response of the Daubechies wavelet at different scales is illustrated in Figure 4(c). With an increasing of the scale, the bandwidth declines. The 3 dB bandwidth of scales $2^1, 2^2$ and 2^3 are 38, 19 and 9 respectively. The frequency range at scales 2^1 and 2^2 is sufficient for processing PPG signals in MIMIC databases. The optimal scale is selected according to the processing effect and computational complexity. A detailed analysis is provided in Section 5.

3 Neural network

Neural network is a powerful tool for nonlinear function estimation owing to its ability to reconstruct complicated signals. Many typical studies have been reported [24–26]. Nevertheless, the application of neural networks suffers from specific issues, including the node function, the number of hidden layers, the number of nodes per layer and the node weight. The reconstruction error is determined by these

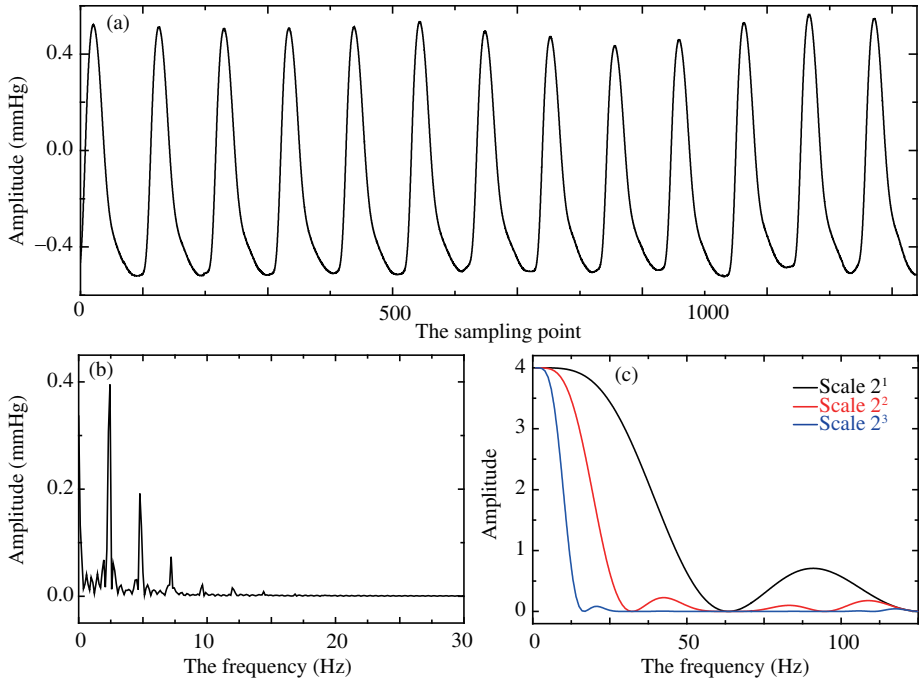

Figure 4 (Color online) (a) Original PPG signals extracted from MIMIC databases; (b) the FFT spectrum analysis of signals in (a); (c) the frequency response of the Daubechies wavelet at different scales.

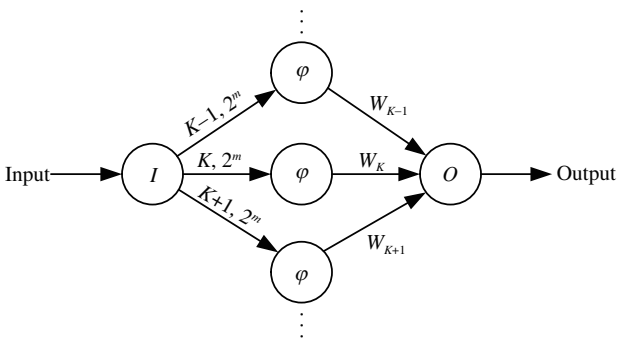

Figure 5 The 3-layer wavelet neural network.

issues. Moreover, the computational complexity is another issue that must be solved carefully and it is determined by the number of hidden layers and the number of nodes per layer. Neural network based on wavelets was first proposed by Zhang and Benveniste [27]. Zhang et al. presented a function learning algorithm based on wavelet neural networks [28]. Subsequently, an optimized wavelet network for multidimensional nonlinear estimation was proposed by Zhang [22].

The objective function $f(t)$ can be approximated by selecting a suitable scale such that

$$f(t) \simeq \sum_k \langle f, \varphi_{mk} \rangle \varphi_{mk}, \tag{3}$$

where m and k are the scale factor and translation factor respectively. $\langle\ ,\ \rangle$ represents the dot product.

A 3-layer wavelet neural network is proposed in [28], as indicated in Figure 5. This design substantially simplifies the structure of the neural network and reduces the computational complexity. Further, the wavelet node function can remove interference and improve the reconstruction accuracy.

However, owing to the large number of hidden layer nodes, it is difficult to apply. Parallel multiplication operations of all hidden layer nodes increase requirements of the necessary processor. The power consumption increases because of the large number of multiplication operations. This paper proposes an optimized wavelet neural network, as presented in Figure 6. Based on the theory in [22], we choose

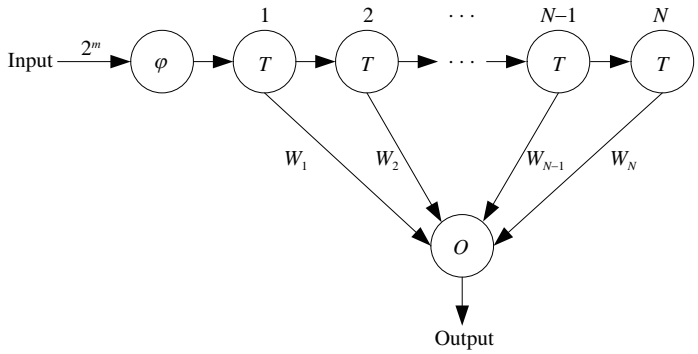

Figure 6 The optimized wavelet neural network.

a single-scaling wavelet basis as the node function. For one-dimensional PPG signals processing, the scale factor s of all wavelet node functions is consistent and the translation factor τ is determined by the threshold k. Therefore, the wavelet node function φ can be reused as indicated in Figure 6, where it is set as the input node function. The output of hidden layer nodes is generated by cache. T represents the cache cycle.

Compared with the structure in Figure 5, the optimized wavelet neural network significantly reduces the computational complexity and the difficulty in application without losing the reconstruction accuracy. The number of multiplication operations is reduced to $1/N$ of that in Figure 5. Using the proposed structure, the increasing of the number of hidden layer nodes results in only a minimal increase of the computational complexity. Without parallel multiplication operations, the power consumption considerably reduced. Furthermore, the implementation of the proposed structure is much easier than that in Figure 5, because the structure of cache hidden layer nodes without multipliers is much simpler than that of wavelet hidden layer nodes.

4 IRBP

The neural network must be trained to minimize the error between the actual and reconstruction curve. Christian et al. improved the resilient backpropagation algorithm to improve the convergence speed [29]. Based on [29], Rusiecki proposed a new solution to remove the outlier error [30]. As analyzed in Subsection 2.2, the low-pass characteristic of Daubechies wavelet node function can remove high-frequency interference, which is presented as outliers in the time domain. Improving the convergence speed is a primary objective of this paper. Through simulation, we determined that reconstruction accuracy is related to the convergence speed. This paper proposes an IRBP to improve the convergence speed and reconstruction accuracy simultaneously.

4.1 Criterion function

To measure the performance of IRBP, criterion functions are presented in this subsection. t_i is the input signal and $f(t_i)$ is the goal function. The estimation residual is defined as

$$r_i = f(t_i) - O_i, \tag{4}$$

where O_i is the estimation of $f(t_i)$.

The mean function (μ) is defined as

$$\mu = \frac{1}{N}\sum_{i=1}^{N}|r_i|. \tag{5}$$

The standard deviation (σ) function is defined as

$$\sigma = \sqrt{\frac{1}{N}\sum_{i=1}^{N}{r_i}^2}. \tag{6}$$

4.2 Theory of IRBP

To simplify the computation, the convergence speed direction of [29] and [30] are adjusted based on the sign of the error derivative and the step-size of convergence speed depends mainly on scaling factors, η [29] and a [30]. The setting of scaling factors has no specific guideline. We have validated these algorithms by adjusting scaling factors and validation results are presented in Figure 7. The gradient of σ represents the convergence speed. As indicated in Figure 7(a), if the step-size is sufficient, the convergence speed is fast and the reconstruction error rapidly declines. However, it oscillates within a certain range and we cannot determine optimal weights (when σ is the least). Conversely, if we reduce the step-size, the convergence speed reduces. The reconstruction error declines extremely slowly and the number of iterations increases sharply. Determining the least σ is difficult. To solve this problem, this paper optimizes algorithms proposed in [29] and [30] and proposed IRBP based on the global error gradient.

The adjustment step-size is computed as

$$\Delta^{(t)} = -\frac{1}{4}\left(\text{sign}\left(\frac{\partial E^{(t)}}{\partial w_i}\right) * \text{abs}\left(\frac{\partial E}{\partial t}\right)\right), \tag{7}$$

where sign$(\cdot)$ is a symbol function and abs$(\cdot)$ is the absolute value of arguments. The t represents the number of iterations and $\frac{1}{4}$ is employed to lower the adjustment speed and avoid reconstruction error oscillation. E represents the standard deviation (σ). In (7), the global reconstruction error gradient $\frac{\partial E}{\partial t}$ is used to adjust the step-size rather than the local reconstruction error partial derivative $\frac{\partial E^{(t)}}{\partial W_i}$. Because the global reconstruction error gradient implies the changing speed of global error (increasing or decreasing) and finding the least global reconstruction error is the other goal of this paper. Incidentally, the adjustment step-size $\Delta^{(t)}$ can be adjusted effectively, which benefits for determining optimal weights.

For each weight, the variable $\Delta {w_i}^{(t)}$ is defined as

$$\Delta {w_i}^{(t)} = \begin{cases} \Delta^{(t)}, & \dfrac{\partial E^{(t)}}{\partial w_i}\dfrac{\partial E^{(t-1)}}{\partial w_i} \geqslant 0, \\ -\Delta {w_i}^{(t-1)}, & \dfrac{\partial E^{(t)}}{\partial w_i}\dfrac{\partial E^{(t-1)}}{\partial w_i} < 0, E^{(t)} > E^{(t-1)}, \\ 0, & \dfrac{\partial E^{(t)}}{\partial w_i}\dfrac{\partial E^{(t-1)}}{\partial w_i} < 0, E^{(t)} \leqslant E^{(t-1)}. \end{cases} \tag{8}$$

The updating criterion is the same as that in [29]. If the sign of $\frac{\partial E^{(t)}}{\partial w_i}$ is the same in consecutive iterations, the $\Delta {w_i}^{(t)}$ is equal to $\Delta^{(t)}$. Conversely, if the sign changes, the $\Delta {w_i}^{(t)}$ will be adjusted according to the global reconstruction error E. The global information plays a more important role in the adjustment of $\Delta {w_i}^{(t)}$, when the local information ($\frac{\partial E^{(t)}}{\partial w_i}$) is inconsistent. Finally, the weight of different nodes is defined as

$${w_i}^{(t)} = {w_i}^{(t-1)} + \Delta {w_i}^{(t)}. \tag{9}$$

Steps of the IRBP are presented as follows:

Step 1 Initialize weights of each node randomly.

Step 2 Reconstruct the goal function.

Step 3 Calculate the global reconstruction error E according to (6).

Step 4 Determine whether E is the minimum. If the global reconstruction error gradient $\frac{\partial E^{(t)}}{\partial t}$ is less than ε ($\varepsilon \ll 0.01$) in consecutive multiple iterations, stop training and determine the optimal weight of each node. Otherwise, go to Step 5.

Step 5 Update the weight of each node according to (7), (8) and (9). Then go to Step 2.

In this algorithm, the maximum number of iterations and the goal reconstruction error are not set because the minimum reconstruction error gradient is set to the stop condition of iterations. In this manner, the number of iterations can be effectively reduced when the reconstruction error cannot attain the intended target.

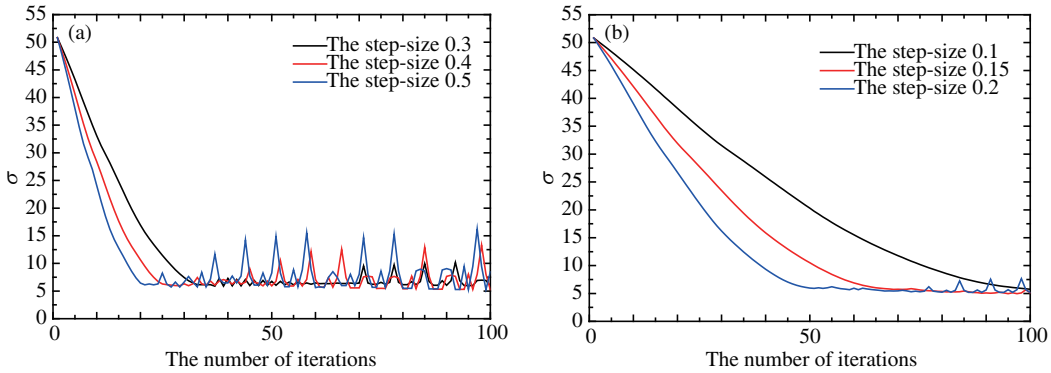

Figure 7 (Color online) The reconstruction error in different number of iterations. The relationship between the number of iterations and the reconstruction error (Long step-size (a) and Short step-size (b)).

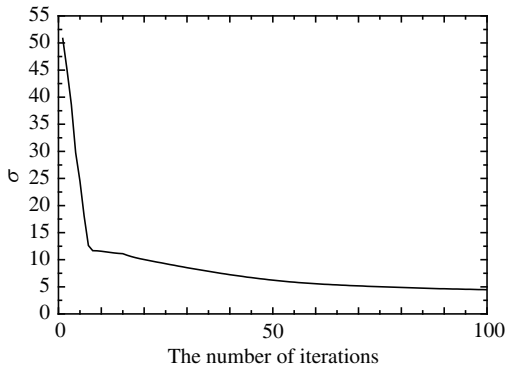

Figure 8 The reconstruction error in different number of iterations.

Experimental results are shown in Figure 8. Compared with [29] and [30], the reconstruction error of this algorithm declines rapidly and stably. It effectively avoids the reconstruction error oscillation as indicated in Figure 7(a) and the number of iterations is much less than that in Figure 7(b). It is a potential option for the calculation of node weights of neural networks.

5 Experiment

The MIMIC database [23] was used to validate the proposed algorithm. The data of more than 90 ICU patients were recorded. Each case contains signals and periodic measurements acquired by a bedside monitor, and some clinical data are acquired from patient's medical records. Fingertip PPG and ABP signals are available in some databases. Some of them are severely contaminated by kinds of noises so that the characteristic of signals has already disappeared. This paper only selects signals whose characteristics are retained.

To begin, the optimal scale of Daubechies wavelet must be selected. Reconstruction error and computational complexity are two primary factors to be considered. As analyzed in Subsection 2.2, the frequency range at scales 2^1 and 2^2 meets the requirement for processing PPG signals in MIMIC databases. Figure 9(a) illustrates the relationship between the reconstruction error and dbs at scales 2^1 and 2^2. For different dbs, the reconstruction error is similar at different scales because the frequency range meets requirements. The tap number of dbs at different scales is presented in Figure 9(b). The number of multiplication operations is proportional to the tap number. From db2 to db6, the computational complexity increases sharply. Therefore, the db2 at scale 2^1 is chosen as the hidden layer node function. For other signals, we can capitalize on the fact that Daubechies wavelet decomposition and the hidden layer node function is selected based on the reconstruction error and computational complexity.

The single-scaling Daubechies wavelet basis improves the robust performance of node function by removing high-frequency interference. The 3-layer wavelet neural network significantly reduces the number

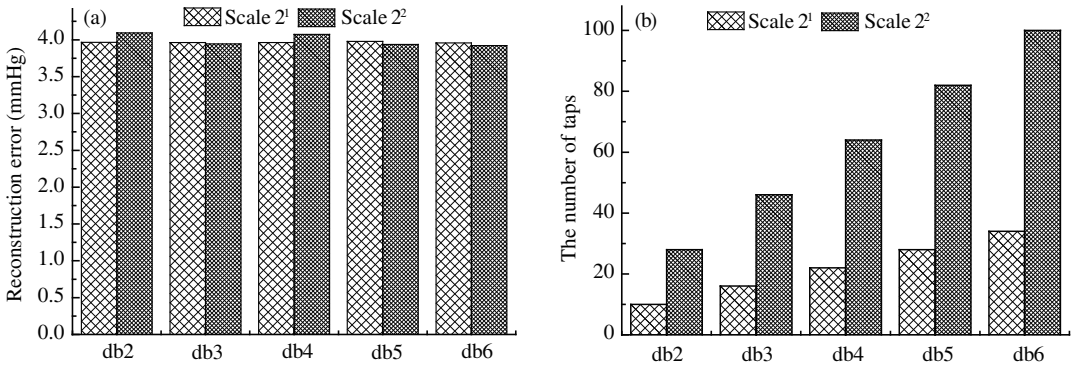

Figure 9 (a) The reconstruction error of dbs at different scales; (b) the tap number of dbs at different scales.

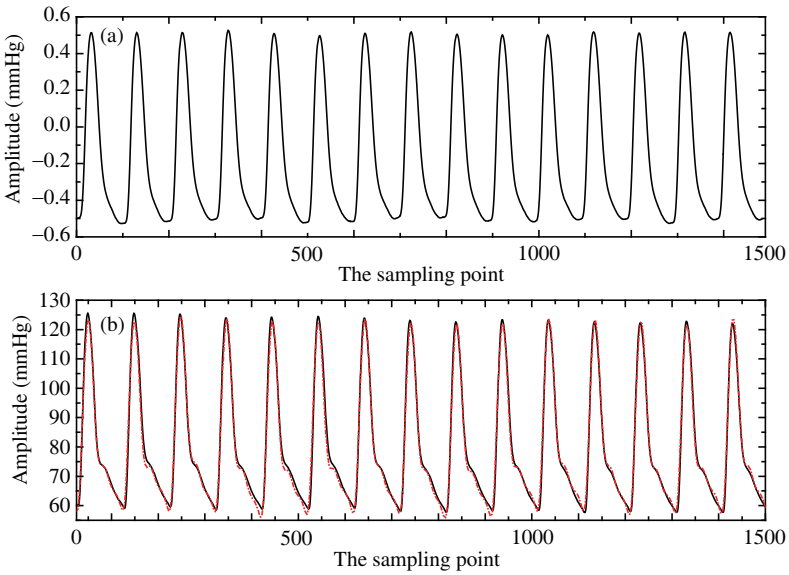

Figure 10 (Color online) The reconstruction result. (a) Input PPG signals (250 Sample/Second, MIMIC databases 230); (b) the original BP and the reconstruction BP (250 Sample/Second, MIMIC databases 230).

Table 1 The reconstruction error of different databases

Reconstruction error	41	55	212	216	218	224	225	230	252
μ (mmHg)	3.9054	3.8999	3.2364	3.0891	3.7245	3.5985	4.0212	2.9658	3.3719
σ (mmHg)	5.1704	4.8242	5.1170	3.9491	4.4337	4.8735	5.6685	4.0761	4.5289

of hidden layers. The optimized structure in Figure 7 addressed the issue that the computational complexity will increase with the increasing in the hidden layer node number. The node weight W_N is of great significance to improve the reconstruction accuracy. The proposed IRBP algorithm improves convergence speed and reduces reconstruction error effectively.

The input wave for network training is part of PPG signals and corresponding BP signals in MIMIC databases. In the training phase, PPG signals are input wave of the wavelet network. Corresponding BP signals and reconstruction signals are used to determine the optimal weights of the wavelet network as indicated in Section 4 (the IRBP algorithm). Finally, the wavelet networks reconstruct another part of BP signals based on corresponding PPG signals in MIMIC databases. Input PPG signals are indicated in Figure 10(a) and corresponding BP signals are presented in Figure 10(b), where the solid line and dotted line are the original and reconstruction BP waveform respectively.

The reconstruction error of different databases is presented in Tables 1 and 2. The average of μ and σ are calculated, which are 3.4094 mmHg and 4.4797 mmHg respectively. In [31], the American National Standards of the Association for the Advancement of Medical Instrumentation is presented. The deviation between measured value and the mercury standard sphygmomanometer must be less than 8 mmHg. All

Table 2 The reconstruction error of different databases

Reconstruction error	253	403	408	437	443	444	466	474	Average
μ (mmHg)	3.8961	3.8912	2.8543	3.9424	2.2896	3.7354	2.6693	2.8613	3.4090
σ (mmHg)	4.9486	4.9173	3.7751	5.2003	2.7778	4.7103	3.1919	3.9929	4.4797

Table 3 Comparisons of different methods

Reference	Method	Algorithm	SBP ($\mu \pm \sigma$)	DBP ($\mu \pm \sigma$)
This work	BP waveform reconstruction	Wavelet neural network	2.32 ± 2.91	1.92 ± 2.47
[20]	Feature extraction	Linear regression	9.8 ± 8.09	5.88 ± 5.11
		neural network (4 inputs)	5.19 ± 5.01	2.91 ± 2.92
		neural network (21 inputs)	3.8 ± 3.46	2.21 ± 2.09
[32]	Feature extraction	Hilbert Huang transform	± 3.85	± 1.84
		Wavelet transform	± 4.17	± 2.57

the σ in Tables 1 and 2 satisfy this criterion.

The SBP and DBP can be extracted from reconstructed BP waveform. Comparisons of different methods are listed in Table 3. (In [32], the calculation method of mean μ is different from that of this paper and [21]. Therefore, the mean μ of [32] is not listed in Table 3). Clearly, most critera of this work are superior to other algorithms'. Comparison results indicate that the proposed algorithm is reliable enough to provide accurate SBP and DBP information for users.

6 Conclusion

A novel wavelet neural network algorithm for continuous and noninvasive BP measurement has been proposed in this paper. Making full use of the low-pass characteristic of Daubechies wavelet, the robustness of hidden layer node function is improved. By reducing large number of parallel multiplication operations, the optimized neural network structure significantly reduces the computational complexity, which facilitates the implementation and application. The IRBP provides detailed method for the adjustment of step-size, which improves convergence speed and lowers the reconstruction error. Validated with the MIMIC database, the average mean squared error σ between reconstructed and actual BP signals is 4.4797 mmHg, which satisfies the American National Standards of the Association for the Advancement of Medical Instrumentation. Medical researchers can extract SBP and DBP from reconstructed BP waveform. The σ of SBP and DBP are 2.91 mmHg and 2.41 mmHA respectively, which are superior to other algorithms'. In addition, by adjusting the Daubechies wavelet according to input signals, the proposed algorithm can be used to reconstruct other waveform. This algorithm provides a new method for BP estimation and is a potential option for nonparametric estimation.

Acknowledgements This work was supported by National Basic Research Program of China (973) (Grant No. 2011CB933203), National Natural Science Foundation of China (Grant Nos. 61474107, 61372060, 61335010, 61275200, 61178051, 81300803), National High-Tech Research & Development Program of China (863) (Grants No. 2014AA032901), Grant for Capital Clinical Application Research with Characteristics (Grants No. Z14110700251-4061).

Conflict of interest The authors declare that they have no conflict of interest.

References

1 Zhang X, Pei W H, Huang B J, et al. A low-noise fully-differential CMOS preamplifier for neural recording applications. Sci China Inf Sci, 2012, 55: 441–452

2 Zhang X, Pei W H, Huang B J, et al. Implantable CMOS neurostimulus chip for visual prosthesis. Sci China Inf Sci, 2011, 54: 898–908

3 Xu Z, Ming L, Bo W, et al. A wide measurement range and fast update rate integrated interface for capacitive sensors array. IEEE Trans Circuits Syst I: Regular Papers, 2014, 61: 2–11

4 Wang Y, Zhang X, Liu M, et al. An implantable sacral nerve root recording and stimulation system for micturition function restoration. IEICE Trans Inform Syst, 2014, 97-D: 2790–2801
5 Hu X H, Zhang X, Liu M, et al. A flexible capacitive tactile sensor array with micro structure for robotic application. Sci China Inf Sci, 2014, 57: 120204
6 Ye Y L, Sheu P C-Y, Zeng J Z, et al. An efficient semi-blind source extraction algorithm and its applications to biomedical signal extraction. Sci China Ser F-Inf Sci, 2009, 52: 1863–1874
7 Wang G, Rao N N, Zhang Y, et al. Atrial fibrillatory signal estimation using blind source extraction algorithm based on high-order statistics. Sci China Ser F-Inf Sci, 2008, 51: 1572–1584
8 An J, Lee J H, Ahn C W. An efficient GP approach to recognizing cognitive tasks from fNIRS neural signals. Sci China Inf Sci, 2013, 56: 109201
9 Li P, Liu M, Zhang X, et al. A low-complexity ECG processing algorithm based on the Haar wavelet transform for portable health-care devices. Sci China Inf Sci, 2014, 57: 122303
10 Zorn E A, Wilson M B, Angel J J, et al. Validation of an automated arterial tonometry monitor using association for the advancement of medical instrumentation standards. Blood Pressure Monitor, 1997, 2: 185–188
11 Miyauchi Y, Koyama S, Ishizawa H. Basic experiment of bloodpressure measurement which uses FBG sensors. In: Proceedings of the IEEE International Conference on Instrumentation and Measurement Technology, Minneapolis, 2013. 1767–1770
12 Newlin D B. Relationships of pulse transmission times to pre-ejection period and blood pressure. Phychophysiology, 1981, 18: 316–321
13 Lane J D, Greenstadt L, Shapiro D. Pulse transit time and blood pressure: an intensive analysis. Phychophysiology, 1983, 20: 45–49
14 Xiaochuan H, Goubran R A, Liu X P. Evaluation of the correlation between blood pressure and pulse transit time. In: Proceedings of the IEEE International Conference on Medical Measurements and Applications Proceedings, Gatineau, 2013. 17–20
15 Chen Y, Wen C, Tao G, et al. Continuous and noninvasive measurement of systolic and diastolic blood pressure by one mathematical model with the same model parameters and two separate pulse wave velocities. Ann Biomed Eng, 2012, 40: 871–882
16 Li Y J, Wang Z L, Zhang L, et al. Characters available in photoplethysmogram for blood pressure estimation: beyond the pulse transit time. Australas Phys Eng Sci, 2014, 37: 367–376
17 Teng X F, Zhang Y T. Continuous and noninvasive estimation of arterial blood pressure using a photoplethysmographic approach. In: Proceedings of the IEEE International Conference on Medicine and Biology Society, Cancun, 2003. 3153–3156
18 Yoon Y, Yoon G. Nonconstrained blood pressure measurement by photoplethysmography. J Opt Soc Korea, 2006, 10: 91–95
19 Fortino G, Giampà V. PPG-based methods for non invasive and continuous BP measurement: an overview and development issues in body sensor networks. In: Proceedings of the IEEE International Conference on Medical Measur, Ottawa, 2010. 10–13
20 Kurylyak Y, Lamonaca F, Grimaldi D. A neural network-based method for continuous blood pressure estimation from a PPG signal. In: Proceedings of the IEEE International Conference on Instrumentation and Measurement Technology, Minneapolis, 2013. 280–283
21 Boggess A, Narcowich F J. A First Course in Wavelets with Fourier Analysis. Hoboken: Wiley, 2001
22 Qinghua Z. Using wavelet network in nonparametric estimation. IEEE Trans Neural Networks, 1997, 8: 227–236
23 George B M, Roger G M. A database to support development and evaluation of intelligent intensive care monitoring. In: Proceedings of the IEEE International Conference on Computers in Cardiology, Indianapolis, 1996. 657–660
24 Hornik K. Multilayer feedforward networks are universal approximators. Neural Netw, 1989, 2: 183–192
25 Barron A. Universal approximation bounds for superpositions of a sigmoidal function. IEEE Trans Inform Theory, 1993, 39: 930–945
26 Poggio T, Girosi F. Networks for approximation and learning. Proc IEEE, 1990, 78: 1481–1497
27 Zhang Q, Benveniste A. Wavelet networks. IEEE Trans Neural Netw, 1992, 3: 889–898
28 Zhang J, Walter G G, Miao Y, et al. Wavelet neural networks for function learning. IEEE Trans Signal Process, 1995, 43: 1485–1497
29 Igel C, Husken M. Empirical evaluation of the improved Rprop learning algorithms. Neurocomputing, 2003, 50: 105–123
30 Rusiecki A. Robust learning algorithm based on iterative least median of squares. Neural Process Lett, 2012, 36: 145–160
31 American National Standard. Electronic or Automated Sphygmomanometers. ANSI/AAMI SP10, Association for the Advancement of Medical Instrumentation, Arlington, 1992
32 Younhee C, Qiao Z, Seokbum K. Noninvasive cuffless blood pressure estimation using pulse transit time and Hilbert-Huang transform instrumentation. Comput Electr Eng, 2013, 39: 103–111